In presenting this thesis as a partial fulfillment of the requirements for an advanced degree from Emory University, I agree that the Library of the University shall make it available for inspection and circulation in accordance with its regulations, governing materials of this type. I agree that permission to copy from, or to publish, this thesis may be granted by the professor under whose direction it was written, or, in his absence, by the Dean of the Graduate School when such copying or publication is solely for scholarly purpose, or publication of, this thesis which involves potential financial gain will not be allowed without written permission.

_____

Cindee Yates

The Counter Cation Effect in the Synthesis and Subsequent Reactivity of Polyoxometalates

By

Cindee Yates

Master of Science

Department of Chemistry

_____

Dr. Craig Hill
Advisor

_____

Dr. Dale Edmondson
Committee Member

_____

Dr. Cora MacBeth
Committee Member

Accepted:

_____

Dean of the Graduate School

_____

Date

The Counter Cation Effect in the Synthesis and Subsequent Reactivity of Polyoxometalates

By

Cindee Yates

Advisor: Craig L. Hill, PhD.

An abstract of
A thesis submitted to the Faculty of the Graduate
School of Emory University in partial fulfillment
of the requirements for the degree of
Master of Science

Department of Chemistry

2008

Abstract

This thesis describes the role of counter cations in the synthesis of polyoxometalates. Chapter one describes the role of a cesium ion and how its concentration can afford two structurally similar palladium silicotungstate crystal structures $Cs_3K_2Na_4[Cs_2K(H_2O)_7Pd^{II}{}_2WO(H_2O)(A\text{-}\alpha\text{-}SiW_9O_{34})_2]\bullet 5H_2O$ (**1**) and $Cs_9Na_5[Pd^{II}{}_3Si_2W_{18}O_{69}]\bullet 20H_2O$ (**2**). This is the first report of having two complexes so closely related by structure where the only difference in preparation is the concentration of counter cation added. Chapter two describes an iron silicotungstate compound $[(CH_3)_2NH_2]_6[\beta\text{-}Fe^{III}{}_2SiW_{10}O_{36}(OH)_2Cl_2]\bullet 8H_2O\bullet 0.5[(CH_3)_2NH_2Cl]$ (**3**) a structurally similar compound to that of a reported literature compound $[(CH_3)_2NH_2)]_5[\beta\text{-}SiFe_2W_{10}O_{36}(OH)_2(H_2O)Cl]\bullet 7H_2O$ (**4**). Compound **3** is formed following the same literature procedure as **4** but by added more tetra ethyl amine hydrochloride counter cation, **3** is formed. Further studies were performed exchange the chloride atoms for azides.

The Counter Cation Effect in the Synthesis and Subsequent Reactivity of Polyoxometalates

By

Cindee Yates

Advisor: Craig L. Hill, PhD.

A thesis submitted to the Faculty of the Graduate
School of Emory University in partial fulfillment
of the requirements for the degree of
Master of Science

Department of Chemistry

2008

-

Table of Contents

List of Figures
List of Tables

Chapter 1 Palladium silicotungstates

Introduction……1
Experimental……..6
Synthesis of $Cs_3K_2Na_4[Cs_2K(H_2O)_7Pd^{II}{}_2WO(H_2O)(A\text{-}\alpha\text{-}SiW_9O_{34})_2]\bullet 5H_2O$**.....6**
Synthesis of $Cs_9Na_5[Pd^{II}{}_3(SiW_9O_{34})_2]\bullet 16H_2O$**.....12**

Results and Discussion……17
Confirmation that structure 1 is the same as that reported by Kortz *et al*.
$Cs_3K_2Na_4[Cs_2K(H_2O)_7Pd^{II}{}_2WO(H_2O)(A\text{-}\alpha\text{-}SiW_9O_{34})_2]\bullet 5H_2O$**……17**
Synthesis and structure of di- and tri- Palladium Sandwich POMs, 1 and 2**…….19**
Effect of Cs^+ countercation in the synthesis of 1 and 2**……21**

Chapter 2 Iron silicotungstate

Introduction……..……25
Experimental……26
Synthesis of $[(CH_3)_2NH_2]_6[\beta\text{-}Fe^{III}{}_2SiW_{10}O_{36}(OH)_2Cl_2]\bullet 8H_2O\bullet 0.5[(CH_3)_2NH_2Cl]$
…27
Results and Discussion……31
Synthesis and structure of iron silicotungstate**……...……31**
Exchange of the two terminally bound chloride ions**……33**

References……34

List of Figures

Figure 1. Combined polyhedral/ball-and-stick representation of $Cs_3K_2Na_4[Cs_2K(H_2O)_7Pd^{II}_2WO(H_2O)(A\text{-}\alpha\text{-}SiW_9O_{34})_2]\bullet 5H_2O$……...8

Figure 2. IR spectrum of $Cs_3K_2Na_4[Cs_2K(H_2O)_7Pd^{II}_2WO(H_2O)(A\text{-}\alpha\text{-}SiW_9O_{34})_2]\bullet 5H_2O$..9

Figure 3. UV-Vis spectrum of $Cs_3K_2Na_4[Cs_2K(H_2O)_7Pd^{II}_2WO(H_2O)(A\text{-}\alpha\text{-}SiW_9O_{34})_2]\bullet 5H_2O$……...10

Figure 4. Kinetic UV-Vis spectrum of $Cs_3K_2Na_4[Cs_2K(H_2O)_7Pd^{II}_2WO(H_2O)(A\text{-}\alpha\text{-}SiW_9O_{34})_2]\bullet 5H_2O$……..10

Figure 5. Cyclic voltammagram for $Cs_3K_2Na_4[Cs_2K(H_2O)_7Pd^{II}_2WO(H_2O)(A\text{-}\alpha\text{-}SiW_9O_{34})_2]\bullet 5H_2O$.....11

Figure 6. Cyclic voltammagram for $Cs_3K_2Na_4[Cs_2K(H_2O)_7Pd^{II}_2WO(H_2O)(A\text{-}\alpha\text{-}SiW_9O_{34})_2]\bullet 5H_2O$, multiple scans taken……12

Figure 7. Combined polyhedral/ball-and-stick representation of $Cs_9Na_5[Pd^{II}_3Si_2W_{18}O_{69}]\bullet 20H_2O$…….15

Figure 8. IR spectrum of $Cs_9Na_5[Pd^{II}_3Si_2W_{18}O_{69}]\bullet 20H_2O$……...…16

Figure 9. UV-Vis spectrum of $Cs_9Na_5[Pd^{II}_3Si_2W_{18}O_{69}]\bullet 20H_2O$…….…17

Figure 10. Kinetic UV-Vis spectra of $Cs_9Na_5[Pd^{II}_3Si_2W_{18}O_{69}]\bullet 20H_2O$...……..17

Figure 11. Cyclic voltammagram for $Cs_9Na_5[Pd^{II}_3Si_2W_{18}O_{69}]\bullet 20H_2O$.....18

Figure 12. Ball-and-stick representation of central belt of $Cs_3K_2Na_4[Cs_2K(H_2O)_7Pd^{II}_2WO(H_2O)(A\text{-}\alpha\text{-}SiW_9O_{34})_2]\bullet 5H_2O$…….…22

Figure 13. Ball-and-stick representation of central belt of $Cs_9Na_5[Pd^{II}_3Si_2W_{18}O_{69}]\bullet 20H_2O$…….23

Figure 14. UV-Vis of batches of $[Pd_{3-x}\{WO(H_2O)\}_x\{A,\alpha\text{-}SiW_9O_{34}\}_2]^{(14-2x)-}$…….....25

Figure 15. Ball-and-stick representation of $[(CH_3)_2NH_2]_6[\beta\text{-}Fe^{III}_2SiW_{10}O_{36}(OH)_2Cl_2]\bullet 8H_2O\bullet 0.5[(CH_3)_2NH_2Cl]$……...……31

Figure 16. IR spectra of $K_8[\gamma\text{-}SiW_{10}O_{38}]\bullet 9H_2O$ and $[(CH_3)_2NH_2]_6[\beta\text{-}Fe^{III}_2SiW_{10}O_{36}(OH)_2Cl_2]\bullet 8H_2O\bullet 0.5[(CH_3)_2NH_2Cl]$……...…...….32

Figure 17. UV-Vis spectra of $[(CH_3)_2NH_2]_6[\beta\text{-}Fe^{III}_2SiW_{10}O_{36}(OH)_2Cl_2]\bullet 8H_2O\bullet 0.5[(CH_3)_2NH_2Cl]$ compared to $[(CH_3)_2NH_2)]_5[\beta\text{-}SiFe_2W_{10}O_{36}(OH)_2(H_2O)Cl]\bullet 7H_2O$……..33

Figure 18. IR spectra of $[(CH_3)_2NH_2]_6[\beta\text{-}Fe^{III}_2SiW_{10}O_{36}(OH)_2Cl_2]\bullet 8H_2O\bullet 0.5[(CH_3)_2NH_2Cl]$ (**3**) in blue, and **3** + azide in red…..36

List of Tables

Table 1. Crystal data and refinement parameters for the X-ray structure of $Cs_3K_2Na_4[Cs_2K(H_2O)_7Pd^{II}{}_2WO(H_2O)(A\text{-}\alpha\text{-}SiW_9O_{34})_2]\bullet 5H_2O$……13

Table 2. Crystal data and refinement parameters for the X-ray structure of $Cs_9Na_5[Pd^{II}{}_3Si_2W_{18}O_{69}]\bullet 20H_2O$……..…19

Table 3. Infrared vibrational bands of $Cs_3K_2Na_4[Cs_2K(H_2O)_7Pd^{II}{}_2WO(H_2O)(A\text{-}\alpha\text{-}SiW_9O_{34})_2]\bullet 5H_2O$……...20

Table 4. Comparison of crystal data and refinement parameters for the X-ray structure of $Cs_3K_2Na_4[Cs_2K(H_2O)_7Pd^{II}{}_2WO(H_2O)(A\text{-}\alpha\text{-}SiW_9O_{34})_2]\bullet 5H_2O$ versus the reported structure of Kortz and co-workers…….21

Table 5. Crystal data and refinement parameters for the X-ray structure of $[(CH_3)_2NH_2]_6[\beta\text{-}Fe^{III}{}_2SiW_{10}O_{36}(OH)_2Cl_2]\bullet 8H_2O\bullet 0.5[(CH_3)_2NH_2Cl]$……..……..34

Table 6. Unit cell comparison from single crystal X-ray diffraction analysis between $[(CH_3)_2NH_2]_6[\beta\text{-}Fe^{III}{}_2SiW_{10}O_{36}(OH)_2Cl_2]\bullet 8H_2O\bullet 0.5[(CH_3)_2NH_2Cl]$, and Botar *et al*.'s published $[(CH_3)_2NH_2)]_5[\beta\text{-}SiFe_2W_{10}O_{36}(OH)_2(H_2O)Cl]$ complex…….……..35

Palladium silicotungstates

Introduction

Polyoxometalates (POMs) are highly tunable discrete molecular units composed of cationic metals bridged by oxide anions.[1] Polyoxometalates usually fall into two classes, isopoly compounds with the general formula of $[M_xO_y]^{n-}$, or, heteropoly compounds with the formula of $[X_zM_xO_y]^{n-}$, where M is typically one of the transition metals, V, Nb, W, and Mo, and X is typically one of the p-block elements but can be one of approximately 60 elements in the periodic table, excluding the noble gases.[2,3] These clusters are highly anionic with charges commonly up to 34- and higher and the predominant oxidized ones (d^0 configuration) are stable towards oxidation. POMs are synthesized from relatively inexpensive and non-toxic materials. This translates into their products generally being environmentally and biologically benign as reported by Hill and co-workers results in their biological studies using POMs as anti-HIV reagents.[4-6] Physically, polyoxometalates are relatively stable polyanions that show selectivity in associating counterions. Additionally, POMs possess extensive catalytic properties. The low cost, benign nature, and reactivities of POMs all contribute to the substantial recent growth in POM research.

The synthesis and challenging task of isolating crystalline forms of polyoxometalates from a solution is of great interest. Since Pope's landmark 1987 chapter in the *Comprehensive Coordination Chemistry*, which highlighted POMs, there have been over 1450 publications on the topic. While a portion of these publications deal with dynamic properties (reactivities, mechanisms, etc.) most of the literature reports on one or multiple novel structures of polyoxometalates. The formation of plenary structures is well known and as of 2004, three volumes of *Inorganic Syntheses* have

included sections that deal with the formation of various POMs.[7-10] R. Villanneau *et al.* have shared with us a manuscript they are working on that reports the rational synthesis of the first series of derivatives, where x = 0, 1, or 2 (see formula above).[11] Knoth and co-workers reported the compound $[Pd_3\{A,\alpha\text{-}PW_9O_{34}\}_2]^{12-}$ (x = 0) along with other $[M_3\{A,\alpha\text{-}PW_9O_{34}\}_2]^{12-}$ complexes, where M = Mn^{2+}, Fe^{2+}, Ni^{2+}, Cu^{2+}, Zn^{2+}, and $\{Ce^{IV}O\}^{2+}$.[12] This more recent work by Villanneau *et al*. demonstrates the possibility to form POMs that are very similar to each other with different starting materials. This, in turn, provides insight on how to further control the synthesis of heteropolyanions.[11]

Once a POM is synthesized, other physical characteristics, like solubility and stability, are of concern for reactivity studies. Since POMs are formed in aqueous solutions, organic solutions, or a mixture thereof, they are soluble and relatively stable in water and organic solvents, as well as thermally stable in the solid state. Further stability is seen upon the photoreduction and new subsequent reoxidations of many POMs by various reactants such as O_2, H^+, 4-chlorophenol,[13] metal ions, and other oxidizers. The stability of POMs in catalytic applications is of great importance, because if a POM falls apart in solution, its catalytic abilities are lost and the reaction mixture will almost certainly be contaminated with POM breakdown products. This makes it nearly impossibly to know what the (true) catalytically active species actually is/are.

POMs frequently display selective reactions with inorganic and organic substrates. The selectivity of polyoxometalates is exhibited, for example by POM cryptates with the formula $[ZP_5W_{30}O_{110}]^{(15-n)-}$ which bind certain lanthanide and other multivalent cations based primarily on ionic radius.[14] Selectivity is also exhibited by POMs in context with separating radionucleotides *via* precipitation or complex

formation. For example, the molybdophosphate anion $\{PMo_{12}\}$ has been used to remove ^{137}Cs, either by precipitation as the tricesium salt or by ion exchange using ammonium or potassium salts.[15,16]

POMs have recently been documented to react with the late-transition-metal elements. Terminal late-transition-metal oxo (LTMO) units have been proposed as intermediates in oxidase enzymes (most frequently in Cu) and for industrial important noble metal catalysts. Such LTMO units could well be intermediates in industrial O_2-based technologies and processes. Catalytic converters (Pt, Pd)[17,18] fuel cell cathodes (Pt, others),[19] and catalysts for low-temperature green O_2-based oxidations (Au, Pt, Pd, Ag, etc.)[15,18] are multi-billion dollar markets. It was long believed that LTMO units were too unstable to be isolated. Due to their instability, their synthesis and isolation of such species has been proven to be a challenging task. However, success has been achieved by using POMs as stabilizing inorganic ligands.

Before 2004, no transition metal to the right of ruthenium on the periodic table had been reported to form a stable terminal oxo unit, except for Wilkinson's $(mesityl)_3Ir^{V}$-oxo complex.[20] In 2004 Anderson *et al.* reported a platinum-oxo species $K_7Na_9[Pt^{IV}(O)(OH_2)(PW_9O_{34})_2]$,[21] and a year later Anderson *et al.* followed up with a terminal palladium-oxo complex $K_{10}Na_3[Pd^{IV}(O)(OH)WO(OH_2)(PW_9O_{34})_2]$.[16] The terminal oxo forms of the coinage metals are much harder to stabilize than platinum and palladium due to their higher d-electron count. However, Cao *et al.* were successful in synthesizing two terminal gold-oxo complexes $K_{15}H_2[Au(O)(OH_2)(PW_9O_{34})_2]\bullet 25H_2O$ and $K_7H_2[Au(O)(OH_2)P_2W_{20}O_{70}(OH_2)_2]\bullet 27H_2O$.[15]

The instability of late transition metal-oxo complexes arises from the increased d-electron count on the metal center, which contributes to the electron population of the terminal M=O unit anti-bonding orbitals.[22-25] The typical C_{4v} terminal M=O unit composed of a d^{0-2} metal will have a bond order of 3. For every added electron to the M=O unit above the d^2 count, the bond order will decrease by ½ as the anti-bonding orbitals are populated. This weakens the M=O bond and activates the oxo ligand.[26] POMs can stabilize terminal oxo forms of some late transition metal elements because they are both good σ donor and π acceptor ligands. A good example is the $[A\text{-}PW_9O_{34}]^{9-}$, a d^0 POM, which has empty, electron-withdrawing W(VI)-based orbitals whose energy and symmetry may reasonably match those of the d-orbitals on the coordinated metal. Upon binding, the electron density in the anti-bonding $d_{xz,yz*}$ orbitals of a terminal metal-oxo unit are delocalized into the empty $d_{xz,yz}$ orbitals of several tungsten centers, thus stabilizing the metal oxo unit.[21]

The only LTMO complexes reported to date utilize phosphorus-centered POM ligands. My research was to create a LTMO complex utilizing silicon-based POM (polytungstate) ligands. Since silicon is invariably Si(IV) and phosphorus in most POMs is the isoelectronic P(V), then any POM containing silicon will be more nucleophilic than its phosphorus complex. I have followed the protocols for preparation of the two palladium LTMO complexes that use phosphorus-centered POMs from Anderson *et al.*[16,21] and Cao *et al.*[15] I used the analogous silicon-centered POMs. These procedures using the silicotungstate resulted in no crystal formation. Kinetic precipitation using KCl or CsCl of these palladium plus silicotungstate POMs syntheses produced an insoluble light brown powder. My objective was to investigate this precipitation process by

varying the reaction conditions to gain a better understanding of the incorporation of palladium into POMs.

To complete an overview of POMs, some of these polyanions are proven to be good catalysts and photocatalysts.[16] POMs may also form the basis of oxdatively stable system for the photocatalytic splitting of water (production of dioxygen and dihydrogen).[26,27]

Today, some of the interesting but difficult challenges in POM chemistry involve the synthesis of fundamentally novel, discrete polyanions. We report here the further analysis of the previously reported structure $Cs_3K_2Na_4[Cs_2K(H_2O)_7Pd^{II}{}_2WO(H_2O)(A\text{-}\alpha\text{-}SiW_9O_{34})_2]\bullet 5H_2O$ (**1**)[27] and the synthesis and characterization of the new silicotungstate transition metal (TM) complex, $Cs_9Na_5[Pd^{II}{}_3(SiW_{18}O_{69})_2]\bullet 16H_2O$ (**2**). These two compounds make up a significant portion of the series of silicon derivatives analogous to the phosphorus-centered Pd complexes of Villanneau et al. discussed above.[11] Compounds **1** and **2** correspond to the di- and tri- palladium species in the series $[Pd_{3-x}\{WO(H_2O)\}_x\{A,\alpha\text{-}SiW_9O_{34}\}_2]^{(14-2x)-}$, where x is found to be 0 and 1, (the x = 2 (mono-palladium) species is still under investigation). Unlike the series of complexes reported by Villanneau *et al.*[11] which uses a different starting material to obtain their products, the partial palladium-silicotungstate based series of complexes reported here is formed from the same starting material, $[A\text{-}\alpha\text{-}SiW_9O_{34}]\bullet 24H_2O$.[28] By merely changing the counter cations, we have demonstrated control over speciation. This is the first reported controlled synthesis of two different complexes performed by only changing the counter cation, allowing us to analyze the counter cation effect in polyoxometalate chemistry. These findings are the basis of a manuscript in preparation.[28]

Experimental

General methods and materials. $Na_{10}[A\text{-}\alpha\text{-}SiW_9O_{34}]\bullet 24H_2O$ was obtained by a published procedure and its identity was confirmed by infrared spectroscopy.[29] Infrared spectra (2% sample in KBr pellet) were recorded on a Nicolet 510 instrument. Elemental analyses of Cs, Na, Si, Pd, and W were performed by Galbraith Laboratories (Knoxville, Tennessee). Electronic absorption spectra were taken on a Hewlett-Packard 8452A UV-Vis spectrophotometer. Electrochemical data were obtained using a BAS CV-50W instrument (Bioanalytical System, Inc.).

Crystallographic studies. Single crystal X-ray crystallographic analyses of **1** and **2** were performed at 173 K on a Bruker D8 SMART APEX CCD sealed tube diffractometer with a graphite monochromated Mo Kα (0.71073 Å) radiation. Data collection, indexing and initial cell refinements were carried out using SMART software (version 5.628). Frame integration and final cell refinements were carried out using SAINT (version 6.36A). Absorption correction was applied using SADABS (version 2.10). The structure was determined using direct methods and difference Fourier techniques. The final R1 scattering factors and anomalous dispersion corrections were taken from the International Tables for X-ray Crystallography. Structure solution, refinement, and generation of publication materials were performed using SHELXTL V6.12 software. Crystal refinement details are listed in Tables 1 and 2.

Synthesis of $Cs_3K_2Na_4[Cs_2K(H_2O)_7Pd^{II}{}_2WO(H_2O)(A\text{-}\alpha\text{-}SiW_9O_{34})_2]\bullet 5H_2O$ (1). A 0.25 g (1.05 mmol) sample of palladium sulfate ($PdSO_4$) was dissolved in 15 mL of acetate buffer (0.25 M $NaOOCCH_3$ and 0.25 M $HOOCCH_3$, pH 4.9) at room temperature and 1.75 g (0.6 mmol) of $Na_{10}[A\text{-}\alpha\text{-}SiW_9O_{34}]\bullet 24H_2O$ was added quickly under vigorous

stirring. After 30-60 seconds, 1.1 mL of 1 M KCl was added dropwise with stirring followed by 1.1 mL of 1 M CsCl added dropwise with stirring. The solution was heated to 60 °C until the solution became clear and was slowly cooled to room temperature on the heat block without stirring. The solution was then filtered using a fine filter paper (Whatman #410). Using slow evaporation, after 1 week small brown blocks of **1** appear (0.4 g, 23%). The crystals were collected by filtration and dried under vacuum (Figure 1).

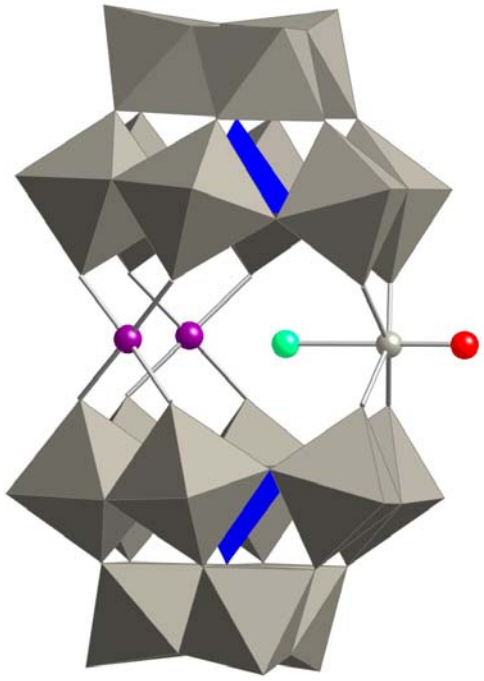

Figure 1. Combined polyhedral/ball-and-stick representation of $Cs_3K_2Na_4[Cs_2K(H_2O)_7Pd^{II}_2WO(H_2O)(A\text{-}\alpha\text{-}SiW_9O_{34})_2]\bullet 5H_2O$ (**1**). The octahedral represent WO_6 (grey) and SiO_4 (blue), and the balls are palladium (purple), oxygen from water (green), and oxygen (red).

IR: Analytical data: IR (2% KBr pellet, 1100 – 400 cm^{-1}): 1001 (s), 940 (s), 889 (vs), 775 (vs), 711 (sh), 585 (sh), 552 (m), 532 (m). Spectrum is shown in Figure 2.

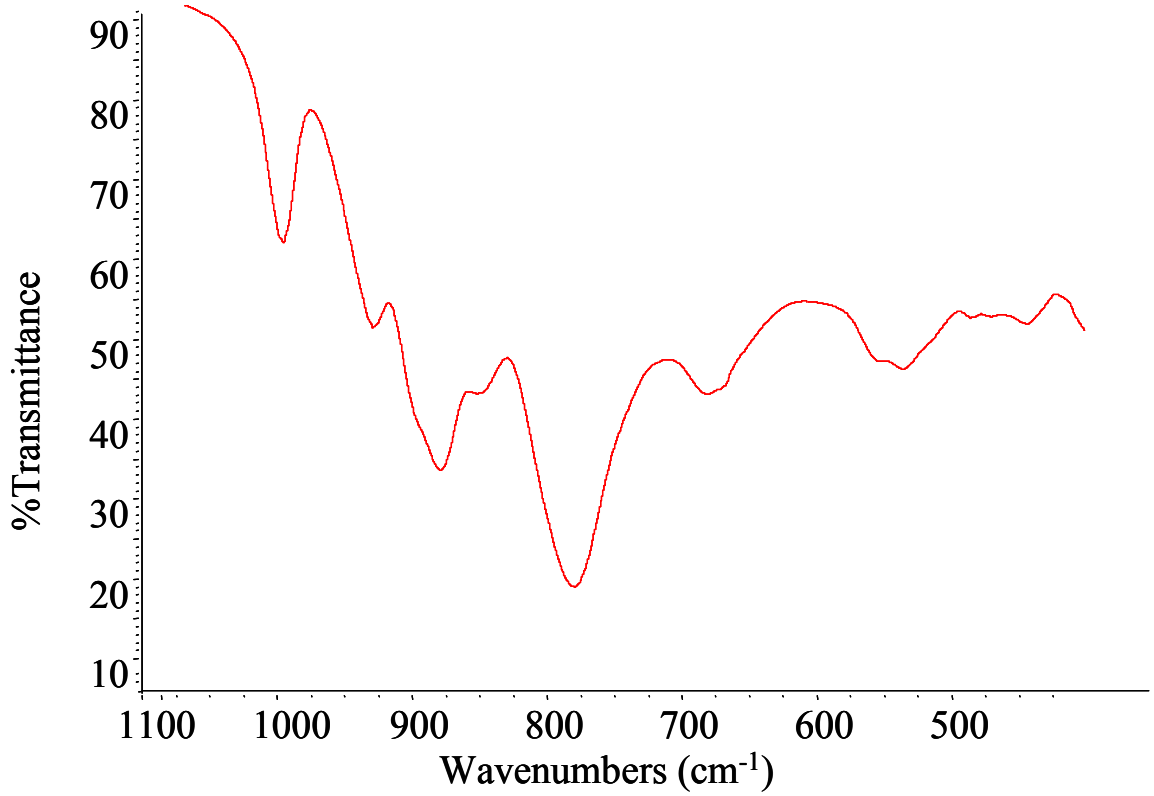

Figure 2. IR spectrum of $Cs_3K_2Na_4[Cs_2K(H_2O)_7Pd^{II}_2WO(H_2O)(A\text{-}\alpha\text{-}SiW_9O_{34})_2]\bullet 5H_2O$ (**1**).

UV-VIS: Electronic spectral data (300 – 800 nm, in H_2O (1.6 mM sample, 1 cm cell path length)) [λ, nm (ε, M^{-1} cm^{-1})]: 440 nm (sh, 379) is shown in Figure 3.

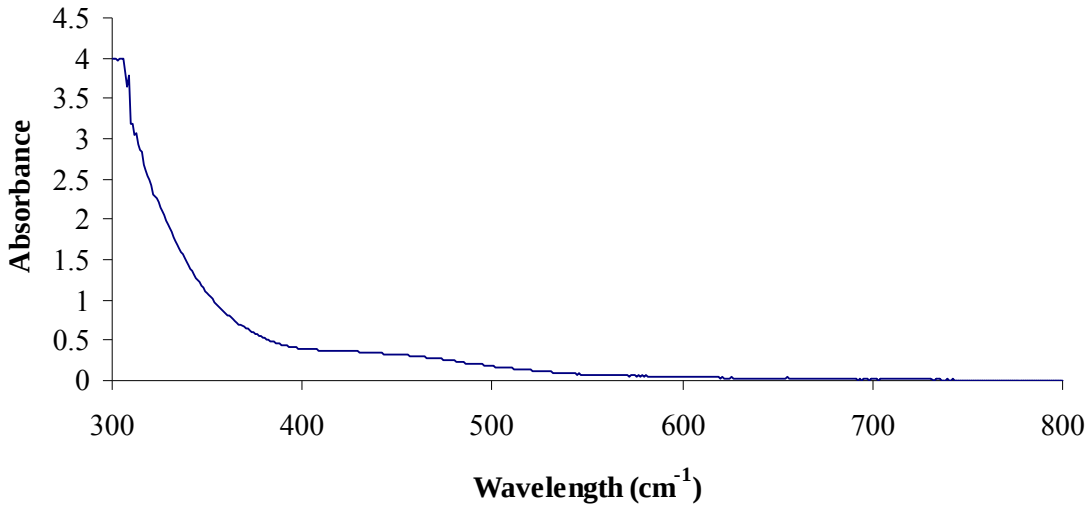

Figure 3. UV-Vis spectrum of $Cs_3K_2Na_4[Cs_2K(H_2O)_7Pd^{II}_2WO(H_2O)(A\text{-}\alpha\text{-}SiW_9O_{34})_2]\bullet 5H_2O$.

Analysis of the UV-Vis results revealed the stability of **1**. Figure 4 below shows the stability of **1** in deionized water over one hour. The spectrum for compound **1** does not change indicating that this POM is stable for this length of time.

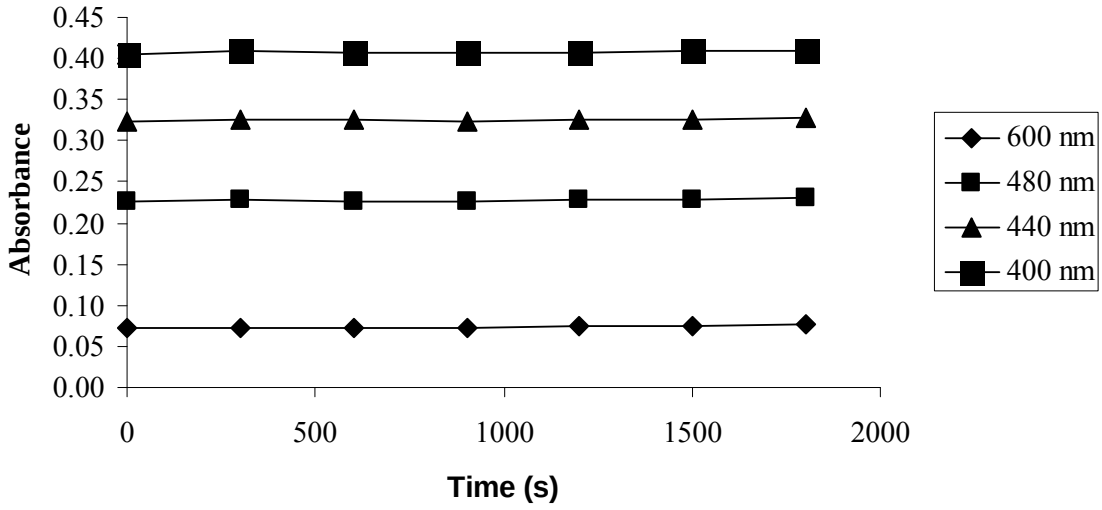

Figure 4. UV-Vis spectrum of $Cs_3K_2Na_4[Cs_2K(H_2O)_7Pd^{II}_2WO(H_2O)(A\text{-}\alpha\text{-}SiW_9O_{34})_2]\bullet 5H_2O$. Samples were taken every 10 minutes for an hour.

Cyclic voltammetry: Pure water was used throughout. Measurements were performed in 0.4 M Na(CH_3COO) + CH_3COOH (pH 5) concentration of **1** was 2 X 10^{-4} M. The solution was then deaerated with pure argon for 10 minutes and kept under positive pressure throughout the experiment. The cyclic voltammagram was recorded at a scan rate of 2 mV•s^{-1} (Figure 5 below).

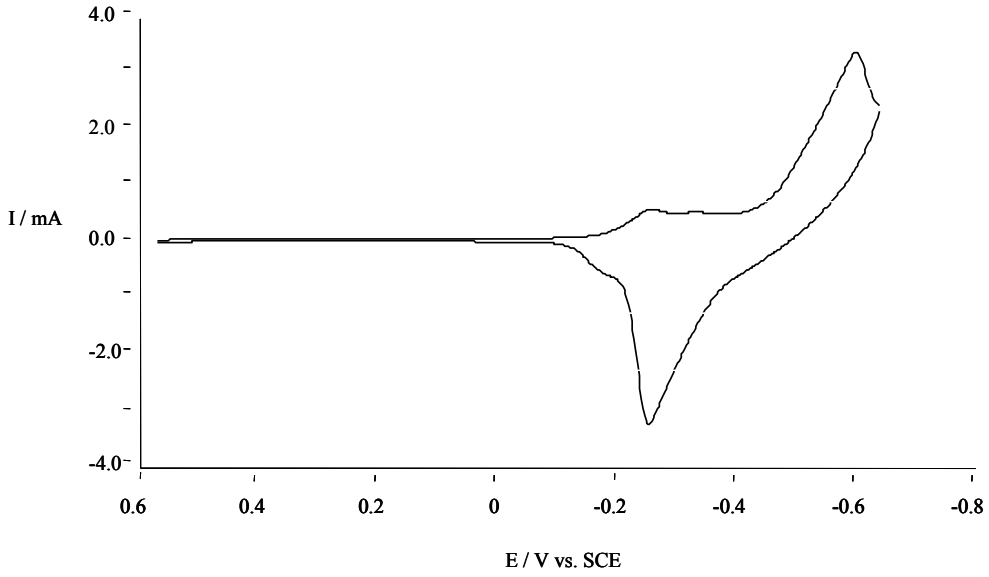

Figure 5. Cyclic voltammagram for **1**.

Consecutive scans from the same sample at a scan rate of 2 mV•s^{-1} showed characteristic deposition behavior of Pd^0 onto a glassy carbon electrode (Figure 6).

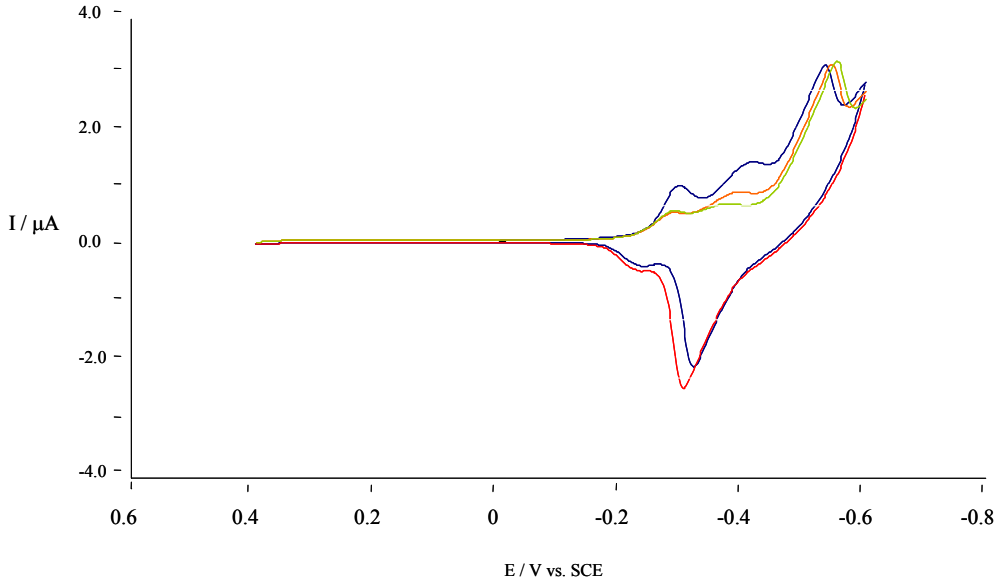

Figure 6. Cyclic voltammagram for **1**, multiple scans taken. Blue is the first scan, red the second, and green the third.

X-ray crystallography: Single crystal crystallographic data are summarized in Table 1.

Table 1. Crystal data and refinement parameters for the X-ray structure of $Cs_3K_2Na_4[Cs_2K(H_2O)_7Pd^{II}{}_2WO(H_2O)(A\text{-}\alpha\text{-}SiW_9O_{34})_2]\bullet 5H_2O$.

	1
molecular formula	$Cs_5H_{26}K_3Na_4O_{82}Pd_2Si_2W_{19}$
formula wt. (g mol^{-1})	5974.06
temperature (K)	173(2)
Radiation (λ, Å)	0.71073
crystal system	Monoclinic
space group	P2(1)/n
A (Å)	16.642(5)
B (Å)	19.615(7)
C (Å)	25.952(8)
β (deg)	95.34(2)
Volume ($Å^3$)	8435(5)
Z	4
ρ_{calcd} (g cm^{-3})	4.677
μ (mm^{-1})	28.637
F(000)	10216
crystal size	0.32 x 0.18 x 0.05
θ range	1.30 to 26.45
index range	$-20 \le h \le 20$ $-24 \le k \le 17$ $-31 \le l \le 32$
Reflections collected	54739
independent reflections	17250 [R(int) = 0.0817]
Absorption correction	semi-empirical from equivalents
max. and min transmission	0.3285 and 0.0394
Refinement method	full-matrix least-squares on F^2
data/restraints/param.	17250/0/655
goodness-of-fit on F^2	1.036
final R indices [$R > 2\sigma$ (I)]	R1 = 0.0781 wR2 = 0.1952
R indices (all data)	R1 = 0.1071 wR2 = 0.2204

[a] $R_1 = \Sigma||F_o| - |F_c||/|F_o|$.

[b] $wR_2 = \{\Sigma[w(F_o^2 - F_c^2)^2]/\Sigma[w(F_o^2)^2]\}^{0.5}$

No elemental analysis was conducted on this complex because all other analysis corresponded with the literature values for the previously published $Cs_3K_2Na_4[Cs_2K(H_2O)_7Pd^{II}{}_2WO(H_2O)(A\text{-}\alpha\text{-}SiW_9O_{34})_2]\bullet 5H_2O$ compound synthesized by Kortz[27] based upon (1) infrared spectroscopy (2) cyclic voltammetry and (3) X-ray single crystal diffraction (the same unit cell and structure) (Table 2 and 3 below). [MW = 5974 g/mol]

Synthesis of $Cs_9Na_5[Pd^{II}{}_3(SiW_9O_{34})_2]\bullet 16H_2O$ (2). A 0.25 g (1.05 mmol) sample of palladium sulfate dihydrate ($PdSO_4{\cdot}2H_2O$) was dissolved and stirred in 15 mL of acetate buffer (0.25 M $NaOOCCH_3$ and 0.25 M $HOOCCH_3$, pH 4.9) at room temperature and 1.75 g (0.6 mmol) of $Na_{10}[A\text{-}\alpha\text{-}SiW_9O_{34}]\bullet 24H_2O$ was added quickly with vigorous stirring. After 30-60 seconds, 2.2 mL of 1 M CsCl was added dropwise with stirring. The solution, with some white suspended precipitate, was heated to 60 °C until the solution clears and was then slowly cooled to room temperature on the heat block without stirring. After cooling, the solution was filtered using a fine filter paper (Whatman #410). The solution was allowed to slowly evaporate and after 12 hours, big brown prisms of **2** appear (0.5 g, 28%). The crystals were collected by filtration and dried under suction (Figure 7).

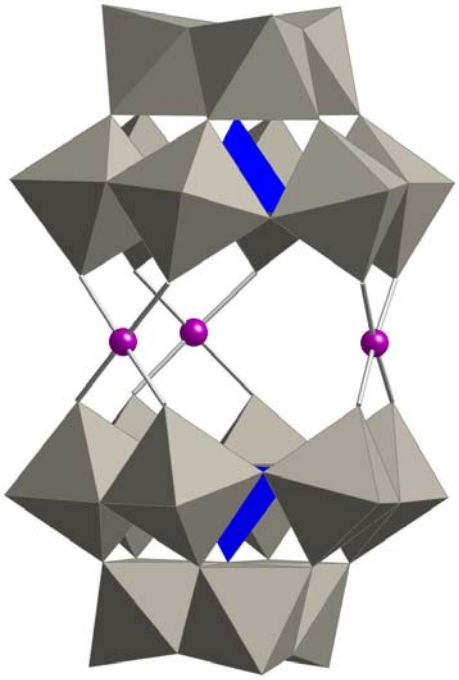

Figure 7. Combined polyhedral/ball-and-stick representation of $Cs_9Na_5[Pd^{II}_3Si_2W_{18}O_{69}]\bullet 20H_2O$ (**2**). The octahedral represent WO_6 (grey) and SiO_4 (blue), and the balls are palladium (purple), oxygen from water (green), and oxygen (red).

IR: Analytical data: IR (2% KBr pellet, 1200 – 400 cm^{-1}): 996 (s), 936 (s), 883 (vs), 778 (vs), 677 (m), 671 (m), 548 (m), 531 (s), and 442 (m). The spectrum is shown below in Figure 8.

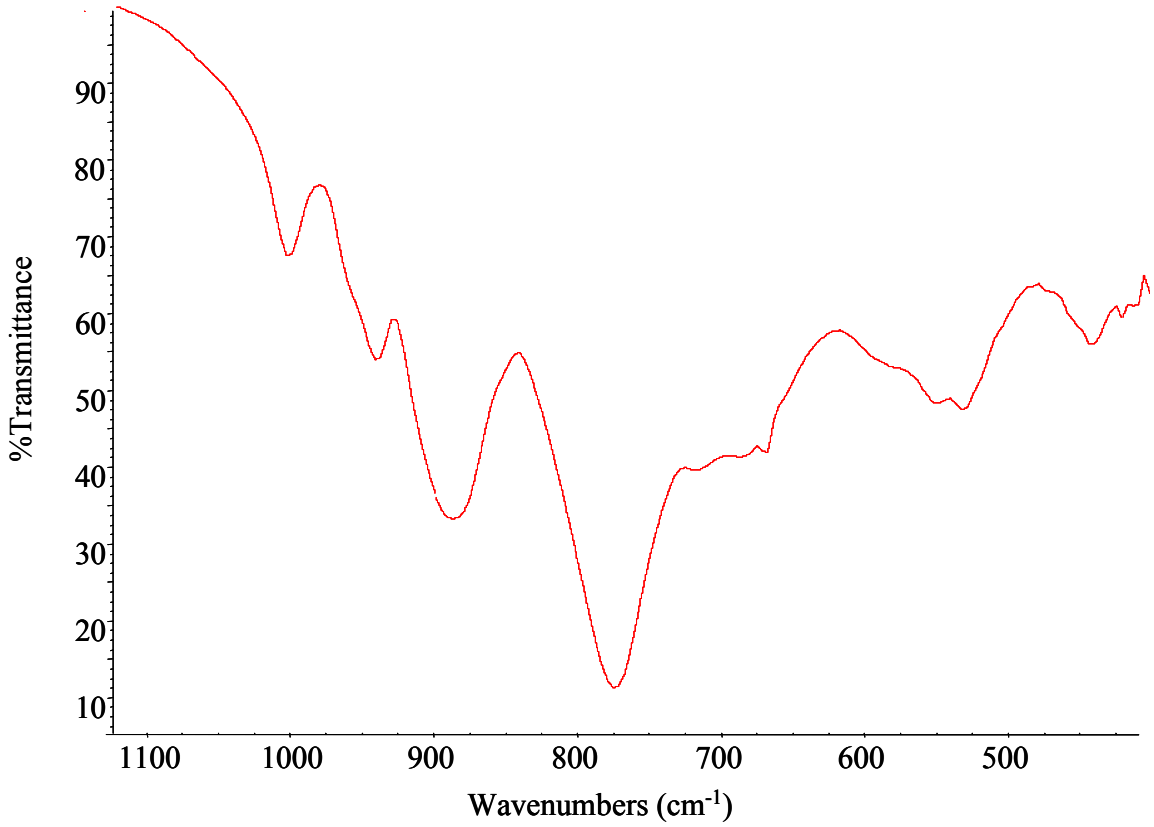

Figure 8. IR spectrum of **2** from 1100 cm^{-1} to 400 cm^{-1}.

UV-Vis: Electronic spectral data (300 – 800 nm, in H_2O (1.6 mM sample in deionized water, 1 cm cell path length)) [λ, nm (ε, M^{-1} cm^{-1})]: 451 nm (574) is shown in Figure 9.

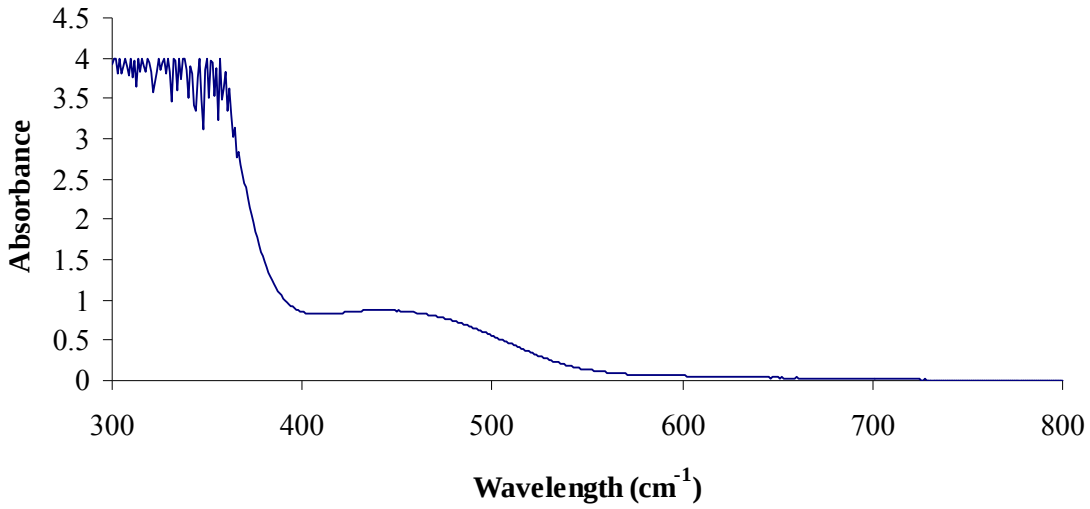

Figure 9. UV-Vis spectrum of $Cs_9Na_5[Pd^{II}_3Si_2W_{18}O_{69}]\bullet 20H_2O$.

Analysis of the UV-Vis results revealed the stability of **2**. Figure 10 below shows the stability of **2** in deionized water over one hour. The spectrum for compound **2** does not change indicating that this POM is stable for this length of time.

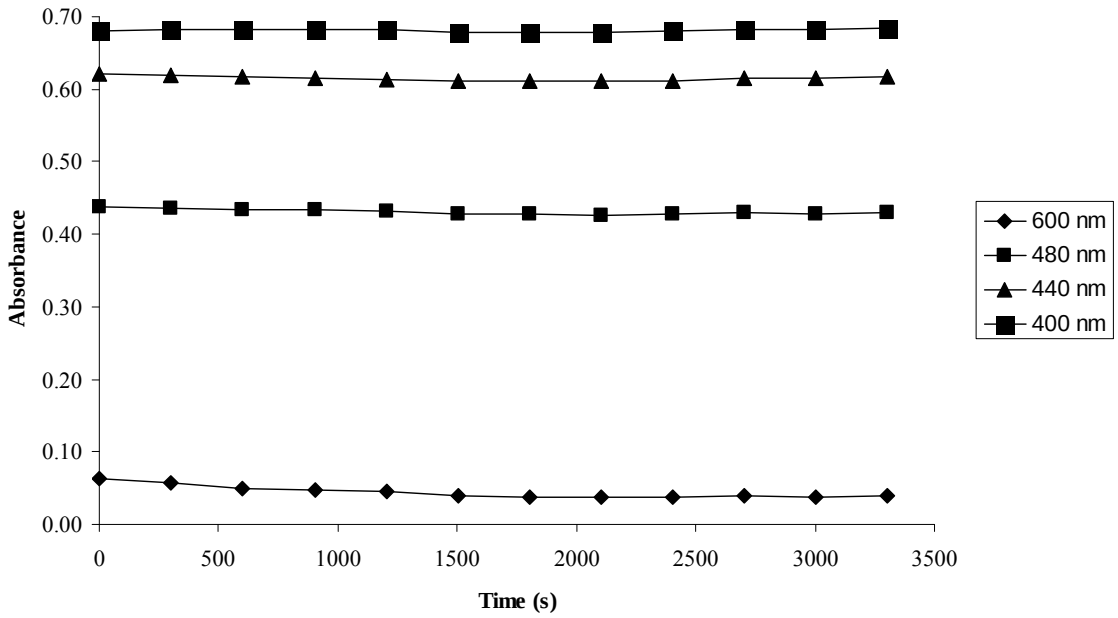

Figure 10. UV-Vis spectra of $Cs_9Na_5[Pd^{II}_3Si_2W_{18}O_{69}]\bullet 20H_2O$. Multiple samples were taken for half an hour.

Cyclic voltammetry: Pure water was used throughout. Measurements were performed in 0.4 M.Na(CH_3COO) + CH_3COOH (pH 5), and concentration of **1** was 2 x 10^{-4} M. The solution was then deaerated with pure argon for 10 minutes and kept under positive pressure throughout the experiment. The cyclic voltammagram was recorded at a scan rate of 2 mV•s^{-1} (Figure 11 below).

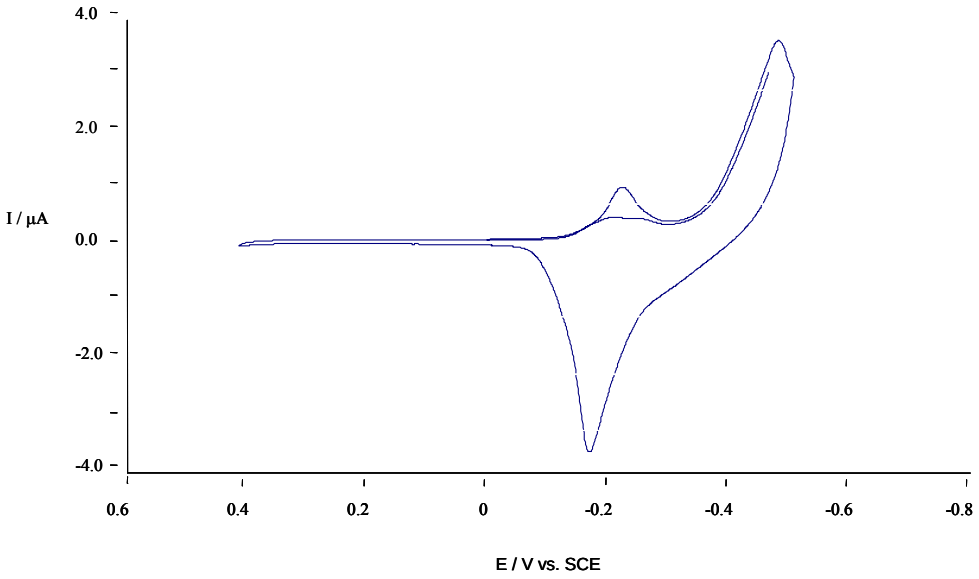

Figure 11. Cyclic voltammagram for **2**.

Electrochemical data at a scan rate 2 mV•s^{-1} shows characteristic deposition behavior of Pd^0 on the glassy carbon electrode when the initial direction was negative. Under the same conditions as above when brought towards cathodic potentials first, a peak shows up at 1.2 mV; which is not yet reproducible.

Elemental analysis: Anal. Calcd. for $Cs_9Na_5[Pd^{II}_3(SiW_{18}O_{69})_2]$•$16H_2O$: Cs, 18.6; Na, 1.80; Si, 0.88; Pd, 5.0; W, 51.9. Found: Cs, 18.6; Na, 1.61; Si, 0.80; Pd, 4.52; W, 50.1. [MW = 6372 g/mol]

X-ray crystallography: Single crystal crystallographic data are summarized in Table 2.

Table 2. Crystal data and refinement parameters for the X-ray structure of $Cs_9Na_5[Pd^{II}_3Si_2W_{18}O_{69}]\bullet 20H_2O$.

	2
molecular formula	$Cs_9H_{40}Na_5Pd_3Si_2W_{18}O_{99}$
formula wt. (g mol^{-1})	6729.94
temperature (K)	173(2)
Radiation (λ, Å)	0.71073
crystal system	Monoclinic
space group	P2(1)/n
A (Å)	16.822(4)
B (Å)	19.784(4)
C (Å)	26.933(6)
β (deg)	99.0(10)
Volume ($Å^3$)	8853(3)
Z	4
ρ_{calcd} (g cm^{-3})	4.534
μ (mm^{-1})	27.348
F(000)	10327
crystal size	0.13 x 0.12 x 0.07
θ range	1.53 to 26.40
index range	$-20 \le h \le 21$ $-24 \le k \le 24$ $-33 \le l \le 30$
Reflections collected	73552
independent reflections	18102 [R(int) = 0.0662]
Absorption correction max. and min. transmission	0.2505 and 0.1252
Refinement method	full-matrix least-squares on F2
data/restraints/param.	18102/0/641
goodness-of-fit on F^2	1.033
final R indices [$R > 2\sigma$ (I)]	R1 = 0.0574 wR2 = 0.1507
R indices (all data)	R1 = 0.0792 wR2 = 0.1641

[a] $R_1 = \Sigma||F_o| - |F_c||/ |F_o|$.

[b] $wR_2 = \{\Sigma[w(F_o^2 - F_c^2)^2]/\Sigma[w(F_o^2)^2]\}^{0.}$

Results and Discussion

Confirmation that structure 1 is the same as that reported by Kortz *et al.* **$Cs_3K_2Na_4[Cs_2K(H_2O)_7Pd^{II}_2WO(H_2O)(A\text{-}\alpha\text{-}SiW_9O_{34})_2]\bullet 5H_2O$.** Verification that complex **1** is the same as the one Kortz *et al*. previously published is found from (1) infrared spectroscopy, (2) matching CV, and (3) X-ray single crystal diffraction (the same unit cell and structure).[27] Table 3 below lists the similar IR peaks that Kortz *et al*. have published along side those found for compound **1**. Note the similarity of the two species. I did not report the two shoulder peaks at 957 and 685 cm^{-1} due to unconvincing evidence from the IR spectrum of **1**. There is the slight appearance of the two shoulder peaks in IR data above but they were not strong enough peaks for me to report.

Table 3. Infrared vibrational bands of $Cs_3K_2Na_4[Cs_2K(H_2O)_7Pd^{II}_2WO(H_2O)(A\text{-}\alpha\text{-}SiW_9O_{34})_2]\bullet 5H_2O$: Comparison between previously reported values and those obtained from our sample **1**.

IR	Kortz *et al*.	**1**
cm^{-1}	1001(m)	1001 (s)
	957 (sh)	
	939 (m)	940 (s)
	892 (s)	889 (vs)
	777 (vs)	775 (vs)
	710 (sh)	711 (sh)
	685 (sh)	
	587 (sh)	585 (sh)
	551 (w)	552 (m)
	533 (w)	532 (m)

The protocol set forth by Kortz *et al*. for the electrochemistry was followed, and our sample had a matching cyclic voltammagram to that published by this group.[27] In addition, consecutive CV scans showed that there is a Pd^0 decomposition process of the complex where the palladium atoms are well-separated from the reduction of the W

centers and plate onto the electrode. This is a similar situation to that in the reports by Kortz and co-workers. The last confirmation of the $Cs_3K_2Na_4[Cs_2K(H_2O)_7Pd^{II}{}_2WO(H_2O)(A\text{-}\alpha\text{-}SiW_9O_{34})_2]\bullet 5H_2O$ was achieved from single crystal X-ray diffraction analysis (Table 4).

Table 4. Crystal data and refinement parameters for the X-ray structure of $Cs_3K_2Na_4[Cs_2K(H_2O)_7Pd^{II}{}_2WO(H_2O)(A\text{-}\alpha\text{-}SiW_9O_{34})_2]\bullet 5H_2O$: sample **1** versus the reported structure of Kortz and co-workers.

Compound	Kortz *et al*.	**1**
crystal system	Monoclinic	Monoclinic
Space Group	P2(1)/n	P2(1)/n
A (Å)	16.655(3)	16.642(5)
B (Å)	19.729(4)	19.615(7)
C (Å)	25.995(5)	25.952(8)
β (deg)	95.46(3)	95.34(2)
Volume (Å^3)	8503(3)	8435(5)
Z	4	4

Both structures were confirmed using a single-crystal diffractometer with Mo Kα (0.71073 Å) radiation and solved using similar programs. As noted, both crystals analyzed have the same monoclinic crystal system, space group, angles, and volume. These three matching methods of determining a crystal structure confirm that species **1** is the same as that reported by the Kortz group published $Cs_3K_2Na_4[Cs_2K(H_2O)_7Pd^{II}{}_2WO(H_2O)(A\text{-}\alpha\text{-}SiW_9O_{34})_2]\bullet 5H_2O$.[27,30]

Synthesis and structure of di- and tri- Palladium Sandwich POMs, 1 and 2. The reaction of $[A\text{-}\alpha\text{-}SiW_9O_{36}]^{10-}$ with 2 equivalents of Pd(II) from $PdSO_4$ in a pH 4.9 buffer solution, under ambient temperature with different counter cations, affords two related structures **1** and **2** (see Figures 1 and 2 above). The di-palladium crystal, **1**, has a $[WO(H_2O)]^{4+}$ moiety in the place of the third palladium in **2**. This tungsten is covalently

bounded by six oxygens. Four oxygens serve as bridges to other tungstens with two in-belt oxygen atoms, one inside (water) and one outside of the central cavity. This sandwich compound would give rise to an idealized C_{2v} symmetry, but the counter cations around the central belt decrease the symmetry to C_1. Complex **1** has two Cs^+ cations in the central belt, with one of them located between the two palladium atoms and the other bridging the oxygens between a palladium (Pd2) and an in-belt tungsten (W19). Additionally, a potassium ion bridges the oxygens from the other palladium-tungsten (Pd1-W19) in the plane (Figure 12).

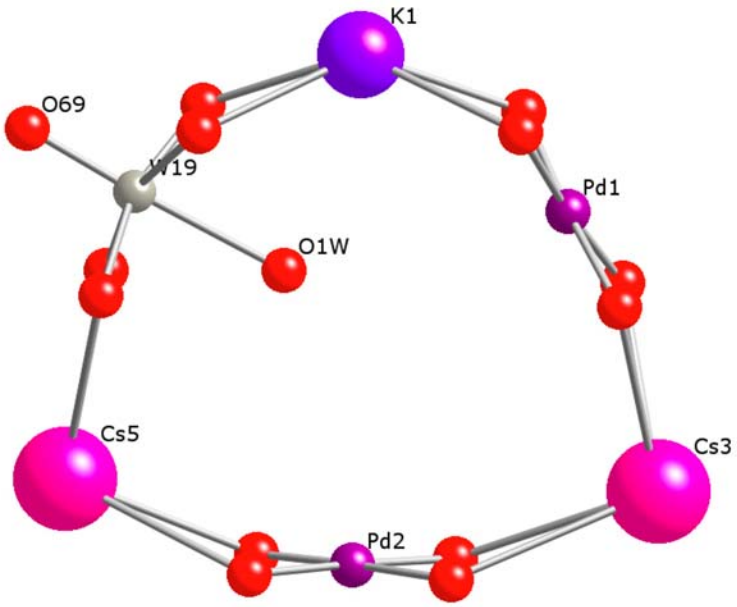

Figure 12. Ball-and-stick representation of central belt of **1**. With cesium (pink), potassium (blue-purple), and O1 water (red).

Even though the overall ionic strengths are the same in both preparations, the latter tri-palladium structure arises when a higher $[Cs^+]/[K^+]$ ratios were used. Complex **2** has alternating Pd and Cs ions with a fourth Cs located in the center of its central

cavity. The three cesium atoms contained within the alternating Pd-Cs ring stabilize the POM. This stabilization is achieved by these in-belt cesium ions binding to four oxygen atoms each, two oxygen atoms from each of the three palladium atoms (Figure 13).

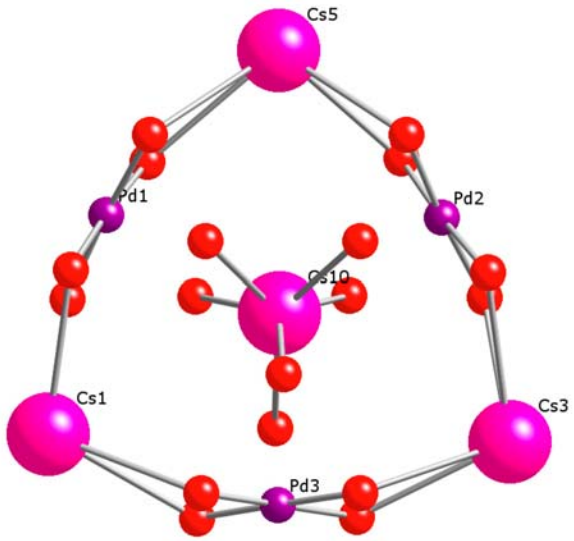

Figure 13. Ball-and-stick representation of central belt of **2**. The color code is the same as Figure 12, with cesium (pink), and potassium (blue-purple).

The innermost cesium ion actually binds to all 12 of the palladium oxygens, further stabilizing the complex. Even with counter-cations accounted for, the tri-palladium symmetrical belt sandwich compound maintains D_{3h} symmetry.

Effect of Cs^+ countercation in the synthesis of 1 and 2. Previous attempts were made to crystallize compounds **1** and **2** without Cs^+. When using potassium as the largest countercation, hexagonal crystals formed that were of too-high symmetry to solve crystallographically. Smaller cations, Na^+ and K^+, fail to stabilize the tri-palladium species. This can be explained by the ion pairing phenomenon. As you move down on the periodic table, the size of the atoms increase, and the interaction between the cation

and the Cl^- anion in solution decreases because the positive cation charge is shielded. The softer cation will therefore be available and more likely to combine with the softer polyanion units. Kortz *et al*. proposed that larger counter-cations are required to stabilize certain POMs and saw the results first hand by his inability to produce complex **1** when starting with the Na^+ salt instead of K^+ salt of the $[A\text{-}\alpha\text{-}SiW_9O_{34}]^{10-}$ anion.[30]

Further work has been performed to synthesize enough of complexes **1** and **2** to perform ^{15}Si NMR. However, any increase of the amounts of the two solutions, reported in experimental above, to gain enough sample for a satisfactory signal-to-noise ^{15}Si NMR spectrum from one batch provides poor X-ray quality crystals. Subsequent batches of **1** and **2** were synthesized in an attempt to combine each type to produce sufficient quantities for the NMR studies. Additionally it was believed that one could distinguish **1** and **2** from examination of their UV-Vis spectra instead of having to take the unit cell. Some batches of type **1** and **2** were confirmed via single crystal X-ray diffraction analysis of the unit cells. Overall, 6 batches were prepared and Figure 14 shows the UV-Vis spectra (300 nm-700 nm) that was taken of them.

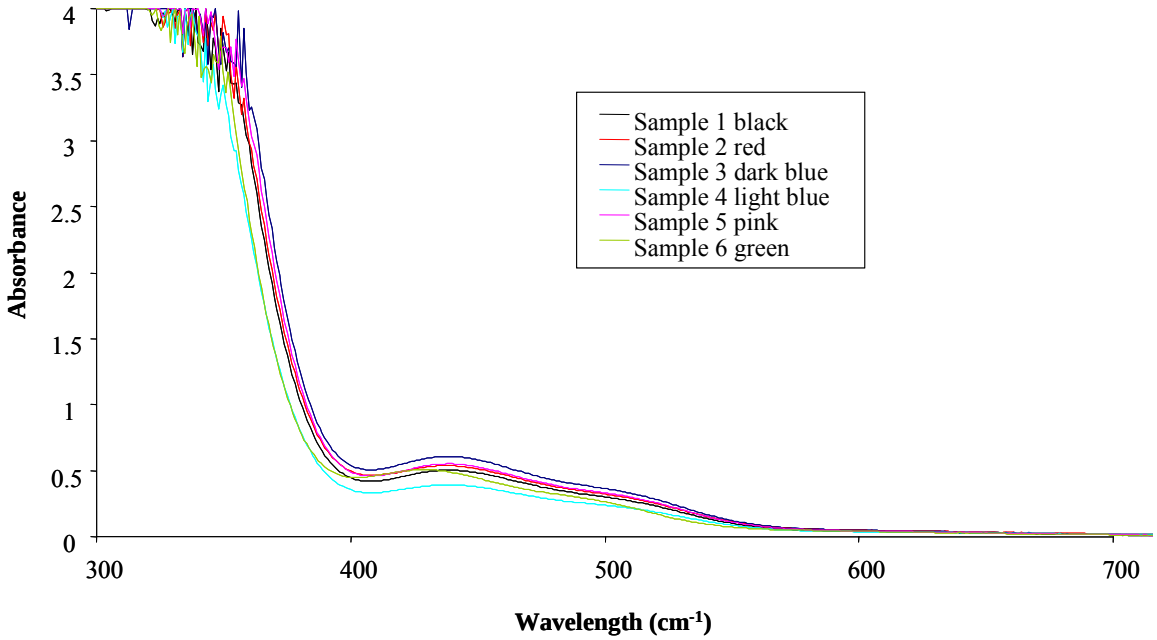

Figure 14. UV-Vis spectra of batches of $[Pd_{3-x}\{WO(H_2O)\}_x\{A,\alpha\text{-}SiW_9O_{34}\}_2]^{(14-2x)-}$, where X is found to be 0 or 1. All samples are made 0.02 g in 2 mL of deionized water. Samples are 1-black, 2-red, 3-dark blue, 4-light blue, 5-pink, and 6-green.

Analysis of the UV-Vis spectra did not show a clear distinction between the two types of crystals. From this, it is believed that from a single solution, both types **1** and **2** precipitate or crystallize.

This series of di- and tri- palladium species is the first known to have controlled speciation from the same starting materials and controlling crystal growth by utilizing the ion pairing effect. Villanneau *et al.* has a manuscript in preparation in which the contents he has shared with our group. He is reporting a series of mono-, di-, and tri- palladium species similar to the ones reported here. However, instead of using the $[A,\alpha\text{-}SiW_9O_{34}]^{10-}$ system, he is utilizing the isostructural phosphorus analogue $[A,\alpha\text{-}PW_9O_{34}]^{9-}$ to flank both sides of the three central palladium centers. In this manuscript, Villanneau *et al*. are able to crystallize the di-, and tri- palladium species from different phosphotungstate precursors, but the mono-palladium species is the only product

identified by elemental analysis. No X-ray quality crystals of the mono-palladium PW_9 series have yet been formed.[11] From this greater understanding of how one can control the synthesis of similar structures, the tunability of polyoxometalates is going to be taken to a higher level. Scientists will be able to better tune POMs for reactivity including selective redox reactions.

Iron silicotungstate

$[(CH_3)_2NH_2]_6[\beta\text{-}Fe^{III}_2SiW_{10}O_{36}(OH)_2Cl_2]\bullet 8H_2O\bullet 0.5[(CH_3)_2NH_2Cl]$

Introduction

The catalytic function of d-electron transition-metal-substituted polyoxometalates has been of great interest to many researchers largely due to the far-reaching acidic and redox properties of this large and growing class of complexes.[2,31-35] For example, Grigoriev *et al.* demonstrated that ion pairing in the exemplary POM, $[\alpha\text{-}SiVW_{11}O_{40}]^{5-}$, can alter the reduction potential, electron accepting ability, and size of the polyanion units in solution.[36] The ability to extensively alter the molecular composition (potentials, charges, sizes, etc.) allows for high tunability in POMs. Therefore, polyoxometalate species exhibit a wide range of reactivities.[1]

Iron is the most abundant transition metal element in the natural world. Iron is found terrestrially, as in minerals,[37,38] biologically, as electron transfer processors,[39] and industrially, such as the Fe(VI) in the ferrate ion, $[Fe^{VI}O_4]^{2-}$ for oxidation in organic synthesis,[40] soil and wastewater treatment,[41,42] batteries,[43] and disinfectants.[44] An advantage of using iron ferrate over other oxidants is that rust (hydrated ferric oxide) is the innocuous reduction product. The disadvantage of this is that ferrate is unstable and usually indiscriminatively reactive. Thus, the synthesis of other high-valent Fe complexes whose reactivity as oxidants can be well-controlled is of particular interest. Work by Berry *et al.* in 2007 has shown that when a low-valent azido complex (Fe(III)-N_3) is photolyzed, an oxidized high-valent iron species Fe(VI)=N is formed.[45] This species is only the second Fe(VI) compound to be structurally characterized, and it is believed it will show greater selective reactivity than ferrate.

In 1999, Mizuno *et al.* reported the iron-containing polyoxometalate, $[\gamma\text{-}SiW_{10}Fe^{III}{}_2O_{38}(H_2O)_2]^{6-}$.[46] Two years later, the same group reported that a solution of the

this complex,[46] is a selective catalyst for the aerobic (air-only) epoxidation of alkenes.[47] Specifically, they reported that $[\gamma\text{-}SiW_{10}Fe^{III}_2O_{38}(H_2O)_2]^{6-}$ POM catalyzes epoxidation under 1 atm of molecular oxygen in the absence of any reducing agents or radical initiator. While subsequent work by our group showed that there is likely no significant role for this POM in the O_2-based epoxidation of the particular substrates they examined,[48] the ability to utilize molecular oxygen is nonetheless of great importance because it has the highest content of active oxygen of all oxidants and its reactions are typically green and inexpensive to conduct. This Fe-containing POM has yet been structurally characterized despite considerable attempts to do so by the Mizuno group, our group and others. Our efforts to react Fe(III) with $[\gamma\text{-}SiW_{10}O_{38}]^{8-}$ in aqueous solution followed by the precipitation with $(CH_3)_2NH_2Cl$, only led to the formation of a new compound, $[(CH_3)_2NH_2]_6[\beta\text{-}Fe^{III}_2SiW_{10}O_{36}(OH)_2Cl_2]\bullet 8H_2O\bullet 0.5[(CH_3)_2NH_2Cl]$ (**3**). Each of the two iron atoms in **3** has a terminal chloride atom. This compound is similar to one reported by Botar *et al*.[48] Since chloride is a reasonably good leaving group, further research focused on exchanging chloride for azide. It was thought that irradiation or heating such terminally bound iron-azide derivatives might lead to high-valent Fe species which might function as more robust functional models for the active sites of some iron-dependent oxygenases such as ribonucleotide reductase (RNR) and methane monooxygenase (MMO).[49]

Experimental

General methods and materials. $K_8[\gamma\text{-}SiW_{10}O_{38}]\bullet 9H_2O$ was obtained by a published procedure and its identity was confirmed by infrared spectroscopy, IR (2%

KBr pellet, 1200 – 400 cm^{-1}): 989 (m), 941 (s), 905 (s), 865 (vs), 818 (vs), 740 (vs), 655 (sh), 553 (w), 528 (m), 478 (sh) (Figure 16).[29]

Infrared spectra (2% sample in KBr pellet) were recorded on a Nicolet 510 instrument. Elemental analyses of C, Cl, Fe, N, Si, and W were performed by Columbia Analytical Services, Tucson, Arizona. Electronic absorption spectra were taken on a Hewlett-Packard 8452A UV-Vis spectrophotometer.

Crystallographic studies. Single-crystal X-ray crystallographic analyses of and **3** was performed at 173 K on a Bruker D8 SMART APEX CCD sealed tube diffractometer with a graphite monochromated Mo Kα (0.71073 Å) radiation. Crystals were mounted on a nylon fiber. Data collection, indexing and initial cell refinements were carried out using SMART software (version 5.628). Frame integration and final cell refinements were carried out using SAINT (version 6.36A). Absorption correction was applied using SADABS (version 2.10). The structure was determined using direct methods and difference Fourier techniques. The final R1 scattering factors and anomalous dispersion corrections were taken from the International Tables for X-ray Crystallography. Structure solution, refinement, and generation of publication materials were performed using SHELXTL V6.12 software.

Synthesis of $[(CH_3)_2NH_2]_6[\beta\text{-}Fe^{III}_2SiW_{10}O_{36}(OH)_2Cl_2]\bullet 8H_2O\bullet 0.5[(CH_3)_2NH_2Cl]$ (3). A 0.275g (0.68 mmol) sample of $Fe(NO_3)_3\bullet 9H_2O$ was dissolved and stirred into 12.5 mL of deionized water at room temperature and 1.0 g (0.34 mmol) of $K_8[\gamma\text{-}SiW_{10}O_{38}]\bullet 9H_2O$ was added quickly with vigorous stirring. The brown iron solution turned yellow with the addition of the POM. Upon clearing of solution (1-2 minutes), solid 6.0 g (73.5 mmol) of

$(CH_3)_2NH_2Cl$ was added in 1 g increments and mixed for 2-3 minutes. Subsequently, 1.0 g of KCl was added with stirring and the resulting solution was filtered with fine filter paper (Whatman #410), leaving a yellow filtrate. The solution was left to slowly evaporate. After 2 days, small pale green crystals of **3** appeared (0.6 g, 89%). The crystals were collected by filtration and dried under suction (Figure 15).

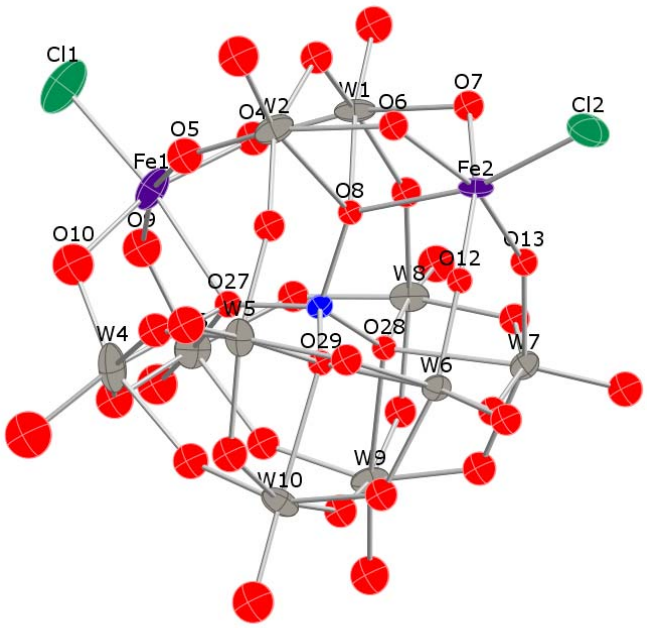

Figure 15. Ball-and-stick representation of $[(CH_3)_2NH_2]_6[\beta\text{-}Fe^{III}{}_2SiW_{10}O_{36}(OH)_2Cl_2]\bullet 8H_2O\bullet 0.5[(CH_3)_2NH_2Cl]$, **3**. Si (blue), Fe (purple), O (red), W (gray), and Cl (green).

IR: Analytical data: IR (2% KBr pellet, 1200 – 400 cm^{-1}): 1018 (s), 991 (s), 957 (s), 900 (s), 881 (sh), 858 (m), 791 (s), 695 (w), 523 (w) (Figure 16).

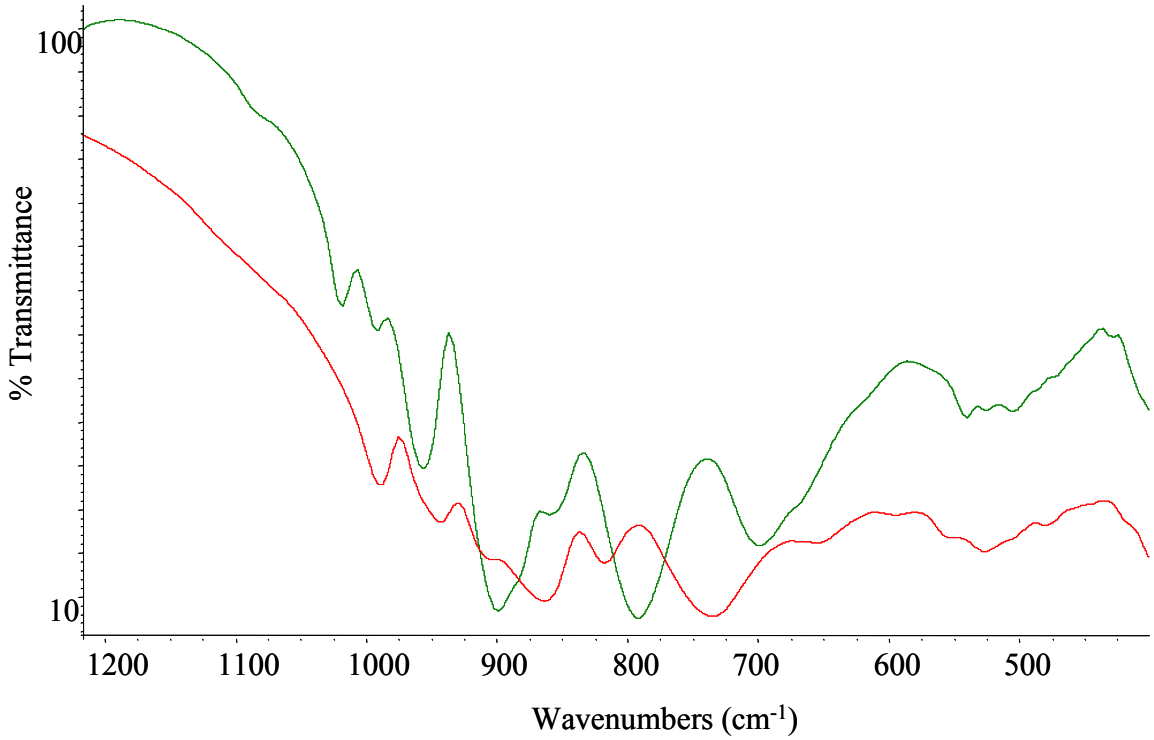

Figure 16. IR spectra of $K_8[\gamma\text{-}SiW_{10}O_{38}]\bullet 9H_2O$ in red and compound **3** in green, both by 2% KBr pellet. Note the shift in peaks of the W-O stretches. This shift is a resultant of an isomerized POM.

UV-Vis: Electronic spectral data (300 – 600 nm, in H_2O (0.5 mM sample, 1 cm cell path length)) [λ, nm (ε, M^{-1} cm^{-1})]: 448 nm (104) (Figure 17).

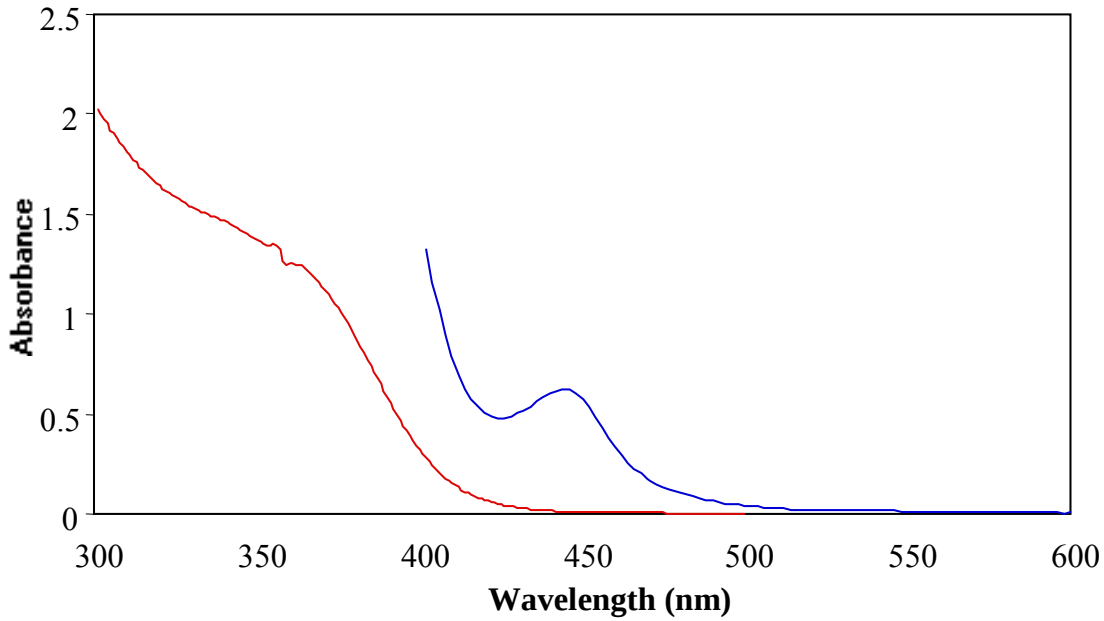

Figure 17. UV-Vis spectra of **3** in red, compared to the iron silicotungstate previously reported by Botar *et al.*, **4** in blue.[48] Note shift in shoulder.

Elemental analysis: Anal. Calcd. for $[(CH_3)_2NH_2]_6[\beta\text{-}Fe^{III}{}_2SiW_{10}O_{36}(OH)_2Cl_2]\bullet 8H_2O\bullet 0.5[(CH_3)_2NH_2Cl]$: C, 5.0; Cl, 2.8; Fe, 3.58; N, 2.92; Si, 0.90; and W, 58.9. Found: C, 4.74; Cl, 3.0; Fe, 3.6; N, 2.72; Si, 1.1; and W, 60.4. [MW = 3102 g/mol]

X-ray crystallography: Crystal refinement details for **3** are listed in Table 5 below.

Table 5. Crystal data and refinement parameters for the X-ray structure of $[(CH_3)_2NH_2]_6[\beta\text{-}Fe^{III}_2SiW_{10}O_{36}(OH)_2Cl_2]\bullet 8H_2O\bullet 0.5[(CH_3)_2NH_2Cl]$.

	3
molecular formula	$C_{13}Cl_2Fe_2H_{70}O_{46}N_{6.5}SiW_{10}$
formula wt. (g mol^{-1})	3102.79
temperature (K)	173(2)
Radiation (λ, Å)	0.71073
crystal system	Monoclinic
space group	P2(1)/n
A (Å)	17.16(12)
B (Å)	16.74(11)
C (Å)	19.30(13)
β (deg)	92.26(2)
Volume ($Å^3$)	5542(6)
Z	4
ρ_{calcd} (g cm^{-3})	3.392
μ (mm^{-1})	21.369
F(000)	4922
crystal size	0.26 x 0.20 x 0.18
θ range	1.56 to 28.33
index range	$-22 \le h \le 22$ $-22 \le k \le 22$ $-25 \le l \le 25$
Reflections collected	83507
independent reflections	13793 [R(int) = 0.0783]
Absorption correction	semi-empirical from equivalents
max. and min. transmission	0.1137 and 0.0720
Refinement method	full-matrix least-squares on F^2
data/restraints/param.	13793/0/356
goodness-of-fit on F^2	1.084
final R indices [R > 2σ (I)]	R1 = 0.0714 wR2 = 0.1713
R indices (all data)	R1 = 0.0865 wR2 = 0.1795

[a] $R_1 = \Sigma||F_o| - |F_c||/ |F_o|$.

[b] $wR_2 = \{\Sigma[w(F_o^2 - F_c^2)^2]/\Sigma[w(F_o^2)^2]\}^0$

Results and discussion

Synthesis and structure of $[(CH_3)_2NH_2]_6[\beta\text{-}Fe^{III}_2SiW_{10}O_{36}(OH)_2Cl_2]\bullet 8H_2O\bullet 0.5[(CH_3)_2NH_2Cl]$ (3).

Reaction of $K_8[\gamma\text{-}SiW_{10}O_{38}]$ with 2 equivalents of Fe(III) from $Fe(NO_3)_3$ in water, at pH 1.7 produces compound **3.** The original $K_8[\gamma\text{-}SiW_{10}O_{38}]$ undergoes a rearrangement in solution from the higher energy gamma- to the more stable beta- form. The monomeric di-iron β-keggin derivative $[(CH_3)_2NH_2]_6[\beta\text{-}Fe^{III}_2SiW_{10}O_{36}(OH)_2Cl_2]\bullet 8H_2O\bullet 0.5[(CH_3)_2NH_2Cl]$, **3**, is representative of the above theory that crystal speciation is controlled by the amount and type of counter cations. This structure is similar to the one previously published by Botar *et al*., $[(CH_3)_2NH_2)]_5[\beta\text{-}SiFe_2W_{10}O_{36}(OH)_2(H_2O)Cl]\bullet 7H_2O$ (**4**).[50] While these two compounds are similar, compound **3** has one chloride atom bound terminally to each iron atom, while compound **4** has one of the chloride atoms replaced by an aqua ligand. The difference in formation between these two crystals is due to the preparatory step where the counter ion $(CH_3)_2NH_2Cl$ is added to **3** at six times the concentration as it is added in **4**. These two compounds, **3** and **4,** are indeed different and that is evident from Figure 17 that compares the UV-Vis spectra of the two complexes. The shift in the shoulder comparing the two samples confirms the complexes are distinct. The differences between these two complexes were also analyzed from the crystallographic evidence. Table 6 below shows the unit cell information for each structure.[50]

Table 6. Unit cell comparison from single crystal X-ray diffraction analysis between $[(CH_3)_2NH_2]_6[\beta\text{-}Fe^{III}{}_2SiW_{10}O_{36}(OH)_2Cl_2]\bullet 8H_2O\bullet 0.5[(CH_3)_2NH_2Cl]$, **3**, and Botar *et al.*'s published $[(CH_3)_2NH_2)]_5[\beta\text{-}SiFe_2W_{10}O_{36}(OH)_2(H_2O)Cl$, **4**.[48]

Compound	**3**	**4**
crystal system	Monoclinic	Monoclinic
Space Group	P2(1)/n	P2(1)/n
A (Å)	17.16(12)	17.09(13)
B (Å)	16.74(11)	15.46(12)
C (Å)	19.30(13)	18.75(15)
β (deg)	92.26(2)	90.34(2)
Volume ($Å^3$)	5542(6)	5224(7)
Z	4	4

In comparing the unit cells (Table 6), it is clear that **3** and **4** while similar are indeed distinct structures. Compound **3** has two chloride atoms bound terminally, one to each of the iron atoms. For some nucleophiles and conditions, chloride can be a better leaving group than aqua, thus it was hoped that exchange reactions might be performed at both chloride sites in **3** but possibly only one site, the chloride site, in **4**.

Exchange of the two terminally bound chloride ions. Exchange of the two chloride ligands by azides is observed by IR spectroscopy (Figure 18).

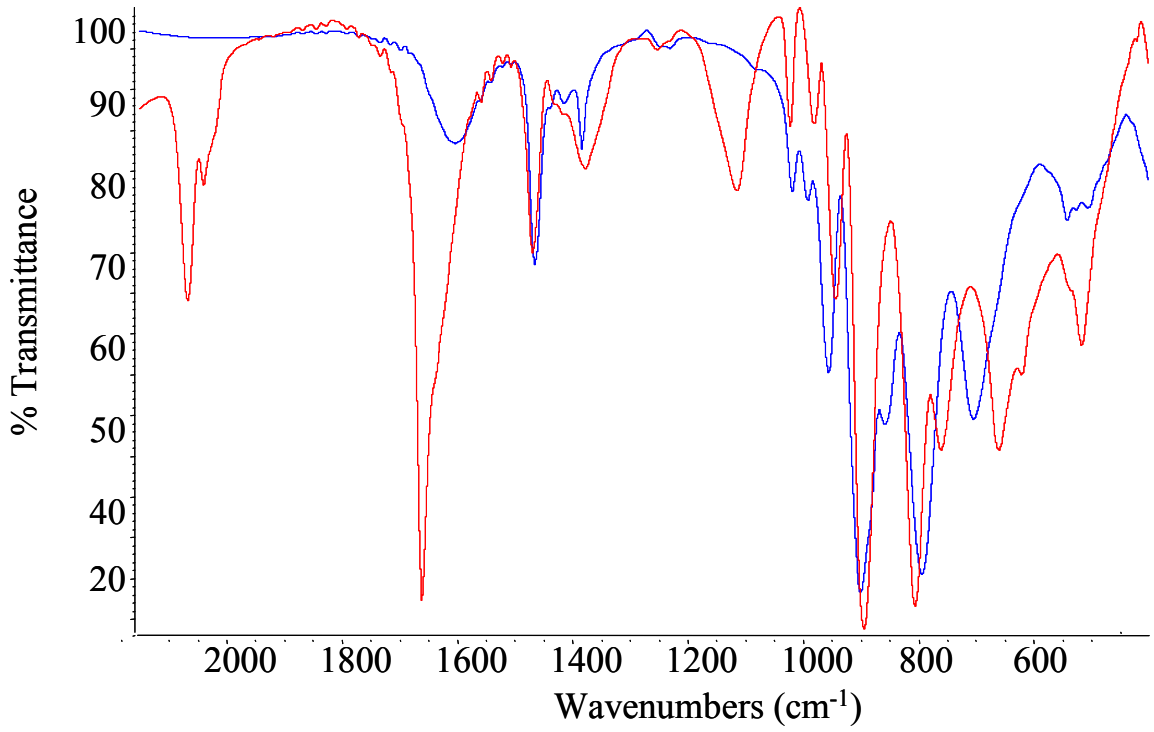

Figure 18. IR spectra of $[(CH_3)_2NH_2]_6[\beta\text{-}Fe^{III}{}_2SiW_{10}O_{36}(OH)_2Cl_2]\bullet 8H_2O\bullet 0.5[(CH_3)_2NH_2Cl]$ (**3**) in blue, and **3** + azide in red. Note the appearance of a bridging azide stretch at 2068cm^{-1}.

A peak appears at 2068 cm^{-1}, which is representative of bound azide. Upon addition of azide into an aqueous solution of **3**, the color changes from a pale yellow to a bright orange in seconds. Precipitation of a powder is done by adding an excess of CsCl. It is still unclear as to how the azide is binding to the iron. The species may be a Fe_1-N_3-Fe_2 bridged dimer or a terminal Fe-N_3 monomer. Isolation of the powder is afforded by centrifugation. Work on crystallizing the powder is still in progress. The ultimate desired structure will be a disorder-free high-valent Fe-nitride POM (with N_2 as by-product from photolysis or thermolysis). Current efforts focus on such transformations.

References

(1) Hill, Craig L. *Chem. Rev.* **1998**, *98*, 1-2.
(2) Pope, M. T.; Müller, A. *Angew. Chem. Int. Ed.* **1991**, *30*, 34-48.
(3) Pope, M. T. In *Comprehensive Coordination Chemistry*; Wilkinson, G.,

Gillard, R. D., Eds.; Pergamon: New York, 1987, 1023-1058.
(4) Judd, D. A.; Nettles, J. H.; Nevins, N.; Snyder, J. P.; Liotta, D. C.; Tang, J.; Ermolieff, J.; Schinazi, R. F.; Hill, C. L. *J. Am. Chem. Soc.* **2001**, *123*, 886-897.
(5) Moskovitz, B. L. *Antimicrob. Agents Chemother.* **1988**, *32*, 1300-1303.
(6) Rhule, J. T.; Hill, C. L.; Judd, D. A.; Schinazi, R. F. *Chem. Rev.* **1998**, *98*, 327-357.
(7) Pope, M. T. In *Comprehensive Coordination Chemistry II: From Biology to Nanotechnology*; Wedd, A. G., Ed.; Elsevier Ltd.: Oxford, UK, **2004**; *4*, 635-678.
(8) Allcock, H. R. *Inorganic Synthesis.* **1985**, *25*, 186-191.
(9) Klemperer, W. G. In *Inorganic Syntheses*; Ginsberg, A. P., Ed.; John Wiley and Sons, Inc.: New York, **1990**; *27*, 71-135.
(10) Nomiya, K.; Pohl, M.; Mizuno, N.; Lyon, D. K.; Finke, R. G. *Inorganic Synthese.s* **1997**, *31*, 186-201.
(11) Villanneau, R., Renaudineau, S., Herson, P., Boubekeur, K., Thouvenot, R., Proust, A. *Personal Communication of unpublished results,* **2008**.
(12) Knoth, W. H.; Domaille, P. J.; Harlow, R. L. *Inorg. Chem.* **1986**, *25*, 1577-1584.
(13) Yue, Bin; Zhou, Yan; Xu, Jingyu; Wu, Zhuzhi; Zhang, Xuan; Zou, Yefen; Jin, Songlin *Environ. Sci. Technol.* **2002**, *36*, 1325-1329.
(14) Creaser, I.; Heckel, M. C.; Neitz, R. J.; Pope, M. T. *Inorg. Chem.* **1993**, *32*, 1573-1578.
(15) Cao, Rui; Anderson, Travis M.; Piccoli, Paula M. B.; Schultz, Arthur J.; Koetzle, Thomas F.; Geletii, Yurii V.; Slonkina, Elena; Hedman, Britt; Hodgson, Keith O.; Hardcastle, Kenneth I.; Fang, Xikui; Kirk, Martin L.; Knottenbelt, Sushilla; Kögerler, Paul; Musaev, Djamaladdin G.; Morokuma, Keiji; Takahashi, Masashi; Hill, Craig L. *J. Am. Chem. Soc.* **2007**, *129*, 11118-11133.
(16) Anderson, Travis M.; Neiwert, W. A.; Kirk, Martin L.; Piccoli, Paula M. B.; Schultz, Arthur J.; Koetzle, Thomas, F.; Musaev, Djamaladdin G.; Morokuma, Keiji; Cao, Rui; Hill, Craig L. *Science* **2004**, *306*, 2074-2077.
(17) Shelef, M. *Chem. Rev.* **1995**, *95*, 209-225.
(18) Singh, Anupam; Sharp, Paul R. *Dalton Trans.* **2005**, 2080-2081.
(19) Appleby, A J.; Foulkes, F. R. *Fuel cell handbook*; Krieger Publising Company, Malabar, Florida, **1993**.
(20) Hay-Motherwell, R. S.; Wilkinson, G.; Hussain-Bates, B.; Hursthouse, M. B. *Polyhedron* **1993**, *12*, 2009-2012.
(21) Anderson, Travis M.; Cao, Rui; Slonkina, Elena; Hedman, Britt; Hodgson, Keith O.; Hardcastle, Kenneth I.; Neiwert, Wade A.; Wu, Shaoxiong; Kirk, Martin L.; Knottenbelt, Sushilla; Depperman, Ezra C.; Keita, Bineta; Nadjo, Louis; Musaev, Djamaladdin G.; Morokuma, Keiji; Hill, Craig L. *J. Am. Chem. Soc.* **2005**, *127*, 11948-11949.
(22) Nugent, W. A.; Mayer, J. M. *Metal-Ligand Multiple Bonds*; John Wiley & Sons, Inc.: New York, **1988**.

(23) Jones, R., Jayaraj, K., Gold, A., Kirk, M.L. *Inorg. Chem.* **1998**, *37*, 2842.
(24) Inscore, F. E.; McNaughton, R.; Westcott, B. L.; Helton, M. E.; Jones, R.; Khawan, I. K.; Enemark, J. H.; Kirk, M. L. *Inorg. Chem.* **1999**, *38*, 1401-1410.
(25) Carducci, M. D., Brown, C., Solomon, E. I., Enemark, J. H. *J. Am. Chem. Soc.* **1994**, *116*, 11856-11868.
(26) Parkin, G. In *Prog. Inorg. Chem.*; Karlin, K. D., Ed.; Wiley: New York, **1998**; *47*, 1-165.
(27) Bi, Li-Hua; Kortz, Ulrich; Keita, Bineta; Nadjo, Louis; Borrmann, Horst *Inorg. Chem.* **2004**, *43*, 8367-8372.
(28) Cao, R., Yates, C., O'Halloran, K., Hardcastle, K.I., Slonkina, E., Hedman, B., Hodgson, K. O., Anderson, T., Hill., C.L. *Manuscript* **2008**.
(29) Tézé, A.; Hervé, G. In *Inorganic Syntheses*; Ginsberg, A. P., Ed.; John Wiley and Sons: New York, **1990**; *27*, 85-96.
(30) Bi, L.-H.; Reicke, M.; Kortz, U.; Keita, B.; Nadjo, L.; Clark, R. J. *Inorg. Chem.* **2004**, *43*, 3915-3920.
(31) Kozhevnikov, I. V. *Chem. Rev.* **1998**, *98*, 171-198.
(32) Mizuno, N.; Misono, M. *Chem. Rev.* **1998**, *98*, 199-218.
(33) Hill, C. L.; Prosser-McCartha, C. M. *Coord. Chem. Rev.* **1995**, *143*, 407-455.
(34) Hill, C. L. *Activation and Functionalization of Alkanes*; John Wiley & Sons: New York, **1989**.
(35) Pope, M. T. *Heteropoly and Isopoly Oxometalates*; Springer-Verlag: Berlin, **1983**.
(36) Grigoriev, V. A.; Cheng, D.; Hill, C. L.; Weinstock, I. A. *J. Am. Chem. Soc.* **2001**, *123*, 5292-5307.
(37) Bowen, L.H., De Grave, E., Vandenberghe, R.E. *Plenum, NY* **1993**, *1*, 115-159.
(38) Murad, E., Johnston, J.H. *Plenum, NY* **1986**, *2*, 507-582.
(39) Beinert, Helmut; Holm, Richard H.; Münck, Eckard *Science* **1997**, *277*, 653-659.
(40) Delaude, L., Laszlo, P. *Journal of Organic Chemistry* **1996**, *61*, 6360.
(41) Sharma, V.K. *Water Sci. Technol.* **2004**, *49*.
(42) Jiang, J.Q., Lloyd, B. *Water Res.* **2002**, *36*, 1397.
(43) Licht, S., Wang, B.H., Gash, S. *Science* **1999**, *285*, 1039.
(44) Kazama, F. *FEMS Microbiol. Lett.* **1994**, *118*.
(45) Berry, John F.; Bill, Eckhard; Bothe, Eberhard; George, Serena DeBeer; Mienert, Bernd; Neese, Frank; Wieghardt, Karl *Science* **2006**, *312*, 1937-1941.
(46) Nozaki, C.; Kiyoto, I.; Minai, Y.; Misono, M.; Mizuno, N. *Inorg. Chem.* **1999**, *38*, 5724-5729.
(47) Nishiyama, Yoshiyuki; Nakagawa, Yoshinao; Mizuno, Noritaka *Angew. Chem. Int. Ed.* **2001**, *40*, 3639-3641.
(48) Botar, B.; Geletii, Y. V.; Kögerler, P.; Musaev, D. G.; Morokuma, K.; Weinstock, I. A.; Hill, C. L. *J. Am. Chem. Soc.* **2006**, *128*, 11268-11277.

(49) Rosenzweig, A. C.; Fredrick, C. A.; Lippard, S. J.; Nordlund, P. *Nature* **1993**, *366*, 537-543.
(50) Botar, Bogdan; Geletii, Yurii V.; Köegerler, Paul; Musaev, Djamaladdin G.; Morokuma, Keiji; Weinstock, Ira A.; Hill, Craig L. *Dalton Trans.* **2005**, 2017-2021.